

Article

Chantriolides F–P, Highly Oxidized Withanolides with Hepatoprotective Activity from *Tacca chantrieri*

Yue Yang^{1,2}, Fei Zhou³, Min Wang^{2,4}, Mukhammadrizo Turanazarov^{2,4}, Xiao-Rong Wang⁵, Changqiang Ke^{1,2}, Sheng Yao^{1,2}, Ligen Lin³ , Chunping Tang^{1,2,*} and Yang Ye^{1,2,4,6,*} 

¹ State Key Laboratory of Drug Research, Shanghai Institute of Materia Medica, Chinese Academy of Sciences, Shanghai 201203, China

² Natural Products Chemistry Department, Shanghai Institute of Materia Medica, Chinese Academy of Sciences, Shanghai 201203, China

³ State Key Laboratory of Quality Research in Chinese Medicine, Institute of Chinese Medical Sciences, University of Macau, Avenida da Universidade, Taipa, Macau 999078, China

⁴ University of Chinese Academy of Sciences, No. 19A Yuquan Road, Beijing 100049, China

⁵ Xishuangbanna Research Institute of Nationality Medicine, Xishuangbanna Hospital of Traditional Dai Medicine, No. 8 Zhuangdong Western Road of Xishuangbanna Tourism and Resort Zone, Xishuangbanna 666100, China

⁶ School of Life Science and Technology, ShanghaiTech University, 393 Middle Huaxia Road, Pudong, Shanghai 201210, China

* Correspondence: tangcp@simm.ac.cn (C.T.); yye@simm.ac.cn (Y.Y.)

Abstract: Eleven highly oxidized withanolides, chantriolides F–P (1–11), together with six known analogues (12–17), were isolated from the rhizomes of *Tacca chantrieri*. Their structures were established on the basis of comprehensive spectroscopic data analysis and comparison with published NMR data, and their absolute configurations were further confirmed by experimental ECD data and single crystal X-ray diffraction analysis. The structures of compounds 5–8 contained a chlorine atom substituted at C-3. Compounds 1 and 12 are a pair of epimers isomerized at C-24 and C-25, while compounds 9 and 16 are isomerized at C-1, C-7, C-24, and C-25. Next, the hepatoprotective effect of all the isolates was evaluated on *tert*-butyl hydroperoxide (*t*-BHP)-injured AML12 hepatocytes. Compounds 5–11 and 16 significantly enhanced cell viability. Compound 8 decreased reactive oxygen species accumulation and increased glutathione level in *t*-BHP injured AML12 hepatocytes through promoting nuclear translocation of nuclear factor erythroid 2-related factor 2 (Nrf2).

Keywords: *Tacca chantrieri*; structural elucidation; withanolides; chantriolides F–P; hepatoprotective effect



Citation: Yang, Y.; Zhou, F.; Wang, M.; Turanazarov, M.; Wang, X.-R.; Ke, C.; Yao, S.; Lin, L.; Tang, C.; Ye, Y. Chantriolides F–P, Highly Oxidized Withanolides with Hepatoprotective Activity from *Tacca chantrieri*. *Molecules* **2022**, *27*, 8197. <https://doi.org/10.3390/molecules27238197>

Academic Editors: Rudolf Bauer and Jelena S. Katanic Stankovic

Received: 24 October 2022

Accepted: 21 November 2022

Published: 24 November 2022

Publisher's Note: MDPI stays neutral with regard to jurisdictional claims in published maps and institutional affiliations.



Copyright: © 2022 by the authors. Licensee MDPI, Basel, Switzerland. This article is an open access article distributed under the terms and conditions of the Creative Commons Attribution (CC BY) license (<https://creativecommons.org/licenses/by/4.0/>).

1. Introduction

Withanolides are a group of highly oxygenated C28-steroidal lactones built on an ergostane skeleton, which are primarily found in the Solanaceae family, particularly in the *Physalis*, *Datura*, *Withania*, and *Nicandra* genera. In addition, withanolides were reported from the Taccaceae, Myrtaceae, Labiataem, Dioscoreaceae, and Asteraceae families, and from the soft corals (marine source) as well. Due to their unique structures [1–5] and diverse biological activities [6–13], withanolides have captured extensive attention, and over the past decade, more than 500 new withanolides of natural origin have been discovered [14–16].

Taccaceae is a family of perennial plants distributed mainly in tropical regions. Chemical investigations revealed the existence of steroids, diarylheptanoids and their glucosides, flavonoids, etc. [17–19]. Of all the isolated compounds, 13 withanolides were characterized from *Tacca subflabellata*, *Tacca plantaginea*, and *Tacca chantrieri*, namely, taccalonolides O and P [20], plantagiolides A–F [21,22], and K–M [23], and chantriolides D and E [24], together with eight withanolide glucosides, including chantriolides A–C [25,26], and E[27], plantagiolides I, J [28], and N [23], and (22*R**,24*R**,25*S**)-3β-[(*O*-β-D-glucopyranosyl-(1→4)-*O*-β-D-glucopyranosyl-(1→2)-*O*-[β-D-glucopyranosyl-(1→6)]-β-D-glucopyranosyl)oxy]-22-hydro

xyergost-5-en-26-oic acid δ -lactone [29]. Most withanolides contain δ -lactone rings by oxidation at C-26 and C-22, while taccalonolides O and P, and chantriolide E bear γ -lactone rings at C-26 and C-23. Plantagiolide I and chantriolide E are two rare withanolide glucosides having a chlorine atom substituted at C-3.

Taccaceae chantrieri is a traditional medicinal plant which has long been used to treat gastric and duodenal ulcers, hepatitis, and hypertension, and it is distributed mainly in Vietnam, Malaysia, Thailand, and southern China. Our previous studies discovered some novel diarylheptanoid dimers from this plant [30], which prompts an in-depth investigation searching for more novel structures with potent bioactivities. A total of 17 withanolides, including 11 new ones, were eventually identified from the rhizomes of *T. chantrieri*. Their structures were determined by extensive analyses of 1D and 2D NMR, HRESIMS data, electronic circular dichroism (ECD) spectra, as well as single-crystal X-ray diffraction studies. All the isolates were evaluated for hepatoprotective effect on *tert*-butyl hydroperoxide (*t*-BHP)-injured AML12 hepatocytes. Herein, the isolation and structure elucidation of new compounds 1–11 and their hepatoprotective activities are presented.

2. Results and Discussion

2.1. Structural Elucidation

Chantriolide F (**1**) was obtained as colorless crystals from acetonitrile. It had a molecular formula of $C_{32}H_{46}O_{11}$ according to the HRESIMS data (m/z 651.3023 ($[M + HCOO]^-$, calcd. for 651.3017), corresponding to 10 indices of hydrogen deficiency. The IR spectrum showed absorption bands for hydroxy (3480 cm^{-1}) and carbonyl groups (1732 cm^{-1}). The ^1H and ^{13}C NMR data (Table 1) of **1** showed characteristics of the withanolide backbone, including four singlet methyls [δ_{H} 1.62, 1.62, 0.77, 0.70; δ_{C} 25.4, 23.7, 16.7, 12.5], one doublet methyl [δ_{H} 1.06 (d, $J = 6.3$ Hz); δ_{C} 12.3], seven oxygenated methines, including two *O*-acetylmethines and two epoxy groups [δ_{H} 5.11 (m), 5.09 (t, $J = 3.4$ Hz), 4.89 (d, $J = 5.7$ Hz), 3.87 (m), 3.54 (dd, $J = 3.7, 1.9$ Hz), 3.11 (t, $J = 2.6$ Hz), 2.95 (d, $J = 3.5$ Hz); δ_{C} 79.7, 76.2, 72.9, 57.0, 55.9, 54.6, 52.0], three oxygenated quaternary carbons (δ_{C} 77.5, 73.6, 70.7), and one ester carbonyl (δ_{C} 179.2). In addition, two acetyl groups (δ_{H} 2.13, 2.04; δ_{C} 170.8, 170.7, 21.5, 20.8) were observed. A detailed analysis of 2D NMR spectra of compound **1** (Figure S1 from Supplementary Materials) further indicated that **1** has the same planar structure (Figure 1) as plantagiolide E (**12**) [21].

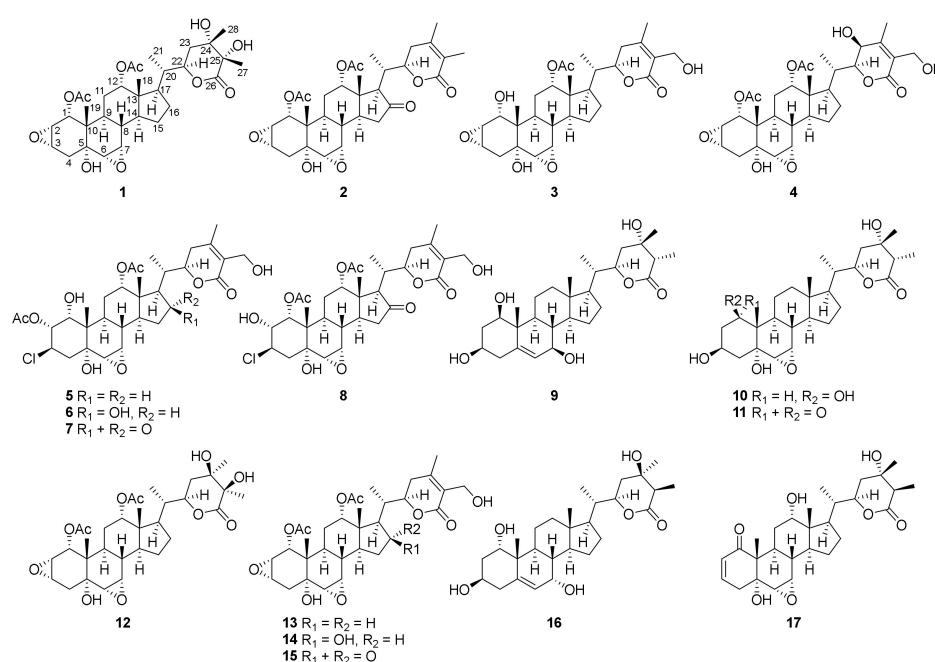


Figure 1. Structures of compounds 1–17 from *Taccaceae chantrieri*.

Table 1. ^1H and ^{13}C NMR data for compounds 1–4 (δ in ppm, J in Hz, in pyridine- d_5).

Position	1^a		2^b		3^b		4^b	
	δ_{C}	δ_{H} (J in Hz)	δ_{C}	δ_{H} (J in Hz)	δ_{C}	δ_{H} (J in Hz)	δ_{C}	δ_{H} (J in Hz)
1	72.9	4.89, d (5.7)	72.8	4.91, d (5.3)	70.4	3.83, m	71.9	4.60, d (5.2)
2	52.0	3.87, m	52.0	3.89, dd (5.2, 3.7)	53.7	3.53, dd (5.6, 3.7)	51.2	3.71, dd (5.2, 3.6)
3	55.9	3.54, dd (3.7, 1.9)	56.0	3.56, dt (3.7, 1.7)	54.1	3.46, t (2.9)	55.2	3.54, dd (3.6, 1.8)
4	33.6	α 2.36, m β 2.08, m	33.6	α 2.38, dd (15.6, 1.5) β 2.08, dd (15.6, 2.1)	34.7	α 2.46, m β 1.99, dd (15.6, 2.5)	32.7	α 2.38, d (15.6) β 2.03, m
5	70.7		70.7		71.8		70.1	
6	57.0	2.95, d (3.5)	57.1	2.98, d (3.6)	57.9	2.94, d (3.7)	56.3	2.83, d (3.6)
7	54.6	3.11, t (2.6)	54.4	3.09, dd (3.6, 2.0)	56.3	3.24, dd (3.7, 2.1)	54.3	3.10, dd (3.6, 2.0)
8	36.8	1.72, m	35.8	1.96, td (11.2, 2.2)	36.7	1.79, m	36.1	1.73, td (11.0, 2.0)
9	28.9	2.42, m	29.2	2.56, m	29.2	2.47, m	28.2	2.02, m
10	40.8		41.0		40.4		40.0	
11	25.2	α 1.79, m β 1.46, td (14.0, 2.4)	24.7	α 1.85, dt (14.4, 3.4) β 1.59, td (14.2, 2.5)	25.8	α 2.45, m β 1.58, m	24.9	1.50, m 1.46, m
12	76.2	5.09, t (3.4)	74.9	5.14, q (3.3)	75.9	5.29, d (3.0)	75.4	4.97, d (2.7)
13	46.6		46.9		46.7		46.2	
14	45.4	2.12, m	40.9	2.62, m	45.8	2.14, m	44.6	2.02, m
15	23.3	1.73, m 1.19, m	37.9	2.51, m 2.15, m	23.4	1.80, m 1.27, m	22.9	1.87, m 1.30, m
16	26.9	1.22, m	216.1		27.1	1.55, m 1.23, m	27.6	1.99, m 1.40, m
17	44.2	1.80, m	56.7	2.67, d (8.7)	44.2	1.78, m	43.9	2.16, m
18	12.5	0.70, s	14.5	0.96, s	12.6	0.73, s	12.0	0.76, s
19	16.7	0.77, s	16.7	0.81, s	15.7	0.69, s	16.4	0.76, s
20	39.0	2.04, m	35.6	2.47, m	39.1	1.92, m	39.5	1.94, m
21	12.3	1.06, d (6.3)	13.2	1.01, d (7.1)	12.9	1.03, d (6.8)	13.6	0.89, d (6.7)
22	79.7	5.11, m	77.7	5.16, m	78.7	4.40, dt (13.2, 3.5)	83.5	4.29, m
23	33.5	2.20, m 2.00, m	31.6	2.25, m 2.14, m	30.1	2.38, dd (17.6, 13.0); 2.05, m	66.7	4.27, m
24	73.6		149.6		154.3		156.2	
25	77.5		122.4		127.9		125.3	
26	179.2		166.7		166.7		165.6	
27	23.7	1.62, s	13.1	1.89, s	56.6	4.87, d (11.7) 4.77, d (11.7)	57.7	4.34, m
28	25.4	1.62, s	20.5	1.74, s	20.5	2.11, s	15.4	2.08, s
1-OAc	20.8	2.13, s	20.8	2.16, s			20.4	2.00, s
12-OAc	170.7		170.8				170.3	
5-OH	21.5	2.04, s	21.7	2.18, s	21.4	1.96, s	21.5	2.06, s
	170.8		170.8		170.5		170.5	
								3.45

^a Recorded at 500 MHz (^1H) and 125 MHz (^{13}C). ^b Recorded at 600 MHz (^1H) and 125 MHz (^{13}C).

In the NOESY spectrum, correlations of H₃-19 with H-1/H-2/H₂-4 β /H-6/H-7/H-8/H₂-11 β , H-8 with H₃-18, and H₃-18 with H₂-11 β /H-12 indicated that they were co-facial and arbitrarily designated as β -oriented. The coupling constant of H-3 (δ_{H} 3.54, dd, J = 3.7, 1.9 Hz) implied that H-3 was on the same face with H-2, and also β -oriented. In addition, NOESY correlations of H-9 with H-14, H-14 with H-17 showed that these protons were α -oriented. The different chemical shifts of compounds **1** and **12** at positions 23, 27 and 28 (**1**: δ_{H} 2.20, m, 2.00, m, 1.62, s, 1.62, s, δ_{C} 33.5, 23.7, 25.4; **12**: δ_{H} 2.84, m, 1.88, m, 1.95, s, 1.79, s, δ_{C} 31.9, 19.4, 24.3) suggested a change in the configuration at positions 24 and 25. The configurations of C-5, C-20, C-21, C-22, C-24, and C-25 were established by single-crystal X-ray diffraction analysis with Cu K α radiation (CCDC 2203317, Figure 2). Therefore, the structure of **1** was identified as the 24*S*, 25*S* epimer of **12**, as shown in Figure 1.

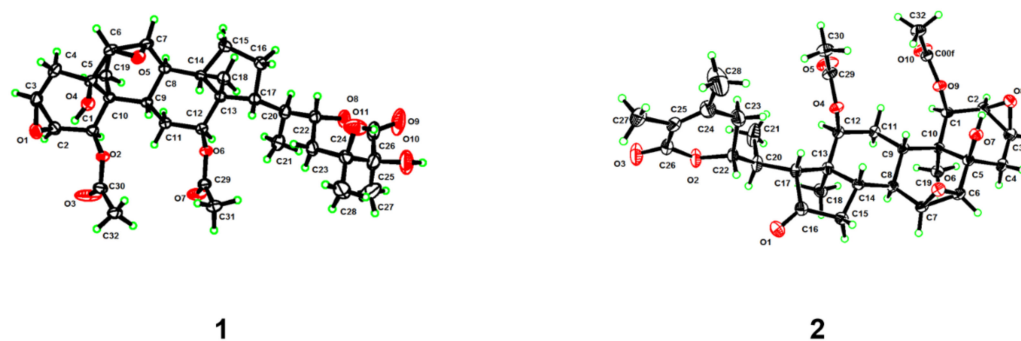


Figure 2. Perspective ORTEP drawings for compounds **1** and **2**.

Compound **2** was isolated as colorless crystals. Its molecular formula, $C_{32}H_{42}O_{10}$, was deduced from the HRESIMS protonated molecular ion at m/z 587.2865 ($[M + H]^+$, calcd. for $C_{32}H_{43}O_{10}$, 587.2856). Its NMR data (Table 1) showed high similarities to those of the known compound plantagiolide A (**15**) [21], except that a methyl (δ_H 1.89; δ_C 13.1) rather than an oxygenated methylene group was observed for **2**. HMBC correlations (Figure S1 from Supplementary Materials) from this methyl to C-24 (δ_C 149.6) and C-26 (δ_C 166.7), and from H₃-28 (δ_H 1.74) to C-23 (δ_C 31.6) and C-25 (δ_C 122.4) suggested the location of the methyl at C-27. The whole structure of **2** was further confirmed by a single-crystal X-ray crystallographic diffraction experiment with Cu K α radiation (CCDC 2203323, Figure 2). Thus, the structure of **2** was proposed as shown, and named chantriolide G.

The molecular formula of **3** was designated by its HRESIMS and ^{13}C NMR data as $C_{30}H_{42}O_9$, which was 42 Da less than that of the known plantagiolide C (**13**) [21]. The proton NMR showed the chemical shift of H-1 of **3** at δ_H 3.83 (m), which was shifted 0.71 ppm upfield compared with that of plantagiolide C, suggesting the miss of acetyl group at C-1. The 1H - 1H COSY correlations (Figure S1 from Supplementary Materials) of H-1/H-2/H-3/H₂-4, and the HMBC correlations from H-1 (δ_H 3.83) to C-5 (δ_C 71.8), and C-10 (δ_C 40.4), from H₃-19 (δ_H 0.69) to C-1 (δ_C 70.4), C-5 (δ_C 71.8), and C-9 (δ_C 29.2) confirmed the assignment. The NOE correlation of H₃-19 and H-1 indicated β -orientation of H-1. The *R*-configuration at the C-22 was confirmed by a positive Cotton effect at 250 nm in the ECD spectrum (Figure 3) of the α,β -unsaturated δ -lactone [31,32]. The same 22*R*-configuration was designated not only for compounds **2** and **3**, but also for compounds **5**–**8** due to the fact that each showed a positive Cotton effect around 250 nm in their ECD spectra. Accordingly, the structure of **3** was proposed as shown and was named chantriolide H.

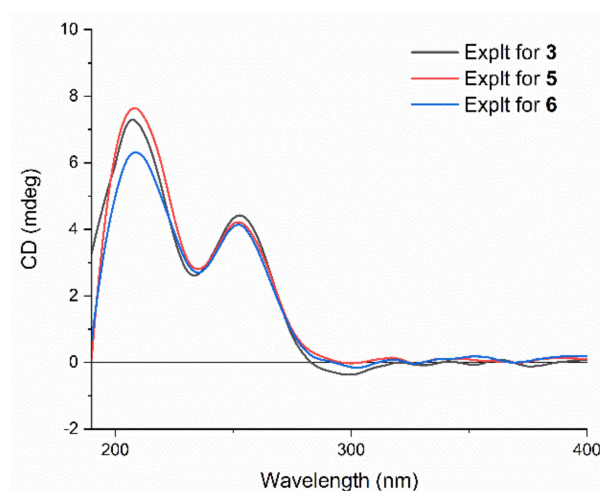


Figure 3. Experimental ECD spectra of compounds **3**, **5**, and **6**.

Chantriolide I (**4**), colorless crystals, had a molecular formula of $C_{32}H_{44}O_{11}$ established by the HRESIMS data (m/z 622.3237 $[M + NH_4]^+$, calcd. for 622.3227) and the ^{13}C NMR data.

Its NMR data (Table 1) also showed high similarities to those of the known plantagiolide C (13) [21] except for the presence of an oxygenated methine [δ_{H} 4.27 (m); δ_{C} 66.7] taking the place of a methylene group in 13. The ^1H - ^1H COSY correlations (Figure S1 from Supplementary Materials) between H-22 (δ_{H} 4.29) and H-23 (δ_{H} 4.27) suggested that the hydroxyl group was located at C-23. The absolute configuration of 4 including the *S*-configuration of C-23 was established by a single-crystal X-ray crystallographic diffraction experiment with Cu $K\alpha$ radiation (CCDC 2203333, Figure 4).

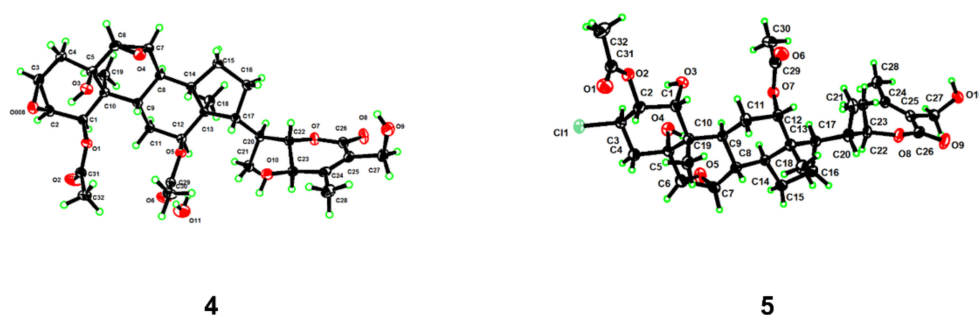


Figure 4. Perspective ORTEP drawings for compounds 4 and 5.

The HRESIMS spectrum of compound 5 showed pseudomolecular ions at m/z 669.2689 and 671.2675 with a ratio being 3:1, indicating the presence of a chlorine atom and a molecular formula of $\text{C}_{32}\text{H}_{45}\text{O}_{10}\text{Cl}$. Such a mass spectral pattern (m/z M:M+2 = 3:1) was also observed for compounds 6–8, suggesting that these compounds also contained a chlorine atom in the molecules. The proton NMR data of 5 (Table 2), almost identical to those of 3 (Table 1), were indicative of a withanolide structure as well, which involved characteristic signals of two acetyl signals at δ_{H} 2.17, 1.94, four methyl signals at δ_{H} 2.11 (s), 1.00 (d, $J = 6.7$ Hz), 0.91 (s), 0.73 (s), two acetylated methine signals at δ_{H} 5.73 (dd, $J = 10.9$, 3.9 Hz), 5.25 (m), two oxygenated methines at δ_{H} 4.40 (dt, $J = 13.2$, 3.5 Hz), 4.09 (dd, $J = 10.0$, 3.9 Hz), two epoxy methine signals at δ_{H} 3.27 (t, $J = 3.0$ Hz), 3.04 (d, $J = 3.7$ Hz), and one oxygenated methylene signal at δ_{H} 4.87 (d, $J = 11.7$ Hz), 4.77 (d, $J = 11.7$ Hz). Compared with 3, compound 5 has one more acetyl group and one chlorine substituted methine. The HMBC correlations (Figure 5) between δ_{H} 5.73 (H-2) and the carbonyl carbon at δ_{C} 171.0 indicate that this acetyl group was located at C-2. In addition, the ^{13}C NMR chemical shift of C-3 (δ_{C} 57.2), together with the ^1H - ^1H COSY correlations of H-1/H-2/H-3/H₂-4, and HMBC correlations from H-1 (δ_{H} 4.09) to C-3 (δ_{C} 57.2), suggested the location of the chlorine atom at C-3. The relative configuration of H-2 and chlorine at C-3 was determined as β by the ROESY correlations of H₃-19/H-2 and OH-1/H-3 (Figure 6). The whole structure of 5 was further confirmed by a single crystal crystallographic diffraction experiment with Cu $K\alpha$ radiation (CCDC 2203335, Figure 4), and named chantriolide J.

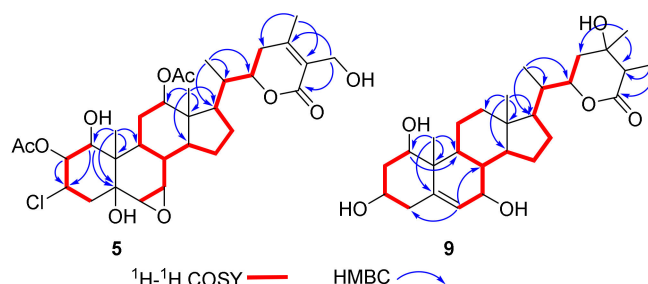
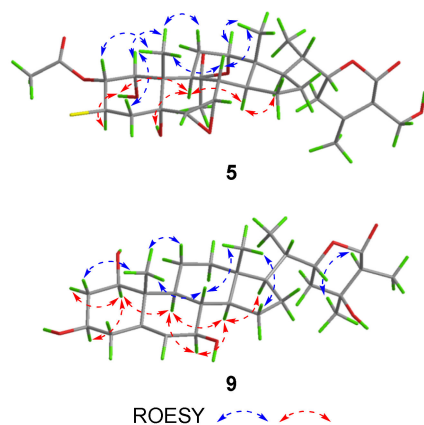


Figure 5. Key ^1H - ^1H COSY and HMBC correlations for compounds 5 and 9.

Table 2. ^1H and ^{13}C NMR data for compounds 5–8 (δ in ppm, J in Hz).

Position	5 ^a		6 ^a		7 ^a		8 ^b	
	δ_{C}	δ_{H} (J in Hz)	δ_{C}	δ_{H} (J in Hz)	δ_{C}	δ_{H} (J in Hz)	δ_{C}	δ_{H} (J in Hz)
1	74.2	4.09, dd (10.0, 3.9)	74.2	4.11, dd (9.9, 4.0)	74.0	4.08, d (3.9)	73.8	5.11, d (4.3)
2	76.9	5.73, dd (10.9, 3.9)	76.9	5.74, dd (11.0, 4.0)	76.9	5.70, dd (10.9, 3.9)	72.8	4.16, dd (10.4, 4.3)
3	57.2	5.12, td (11.5, 5.5)	57.3	5.12, td (11.5, 5.4)	57.2	5.10, m	58.9	4.48, td (11.9, 5.0)
4	44.1	α 2.57, dd (13.3, 5.5) β 2.40, dd (14.6, 10.6)	44.1	α 2.58, m β 2.41, dd (13.3, 12.0)	44.0	α 2.55, m β 2.39, dd (13.3, 11.9)	42.2	α 2.37, m β 2.15, m
5	74.5		74.5		74.5		71.0	
6	56.9	3.04, d (3.7)	57.0	3.05, d (3.7)	56.9	3.04, d (3.7)	57.5	3.05, d (3.7)
7	56.0	3.27, t (3.0)	56.0	3.31, t (3.1)	55.7	3.24, t (3.0)	56.5	3.26, t (3.0)
8	36.1	1.82, m	35.9	2.01, m	35.1	2.06, dd (11.1, 2.4)	34.8	2.03, m
9	30.1	2.51, ddd (14.1, 11.3, 3.5)	30.4	2.54, m	30.3	2.68, m	29.6	1.98, dd (9.9, 6.4)
10	41.8		41.8		41.9		41.9	
11	25.7	α 2.21, dt (14.2, 3.3) β 1.45, td (14.0, 2.8)	25.4	α 2.25, m β 1.56, td (13.8, 2.7)	25.2	α 2.27, m β 1.58, td (13.9, 2.6)	24.3	1.60, m
12	75.7	5.25, m	76.1	5.32, m	74.3	5.31, m	74.5	5.04, d (2.9)
13	46.9		47.0		47.3		46.8	
14	45.8	2.11, m	44.3	2.13, m	41.1	2.60, m	40.0	2.41, m
15	23.3	α 1.83, m β 1.31, dd (12.3, 5.6)	37.1	α 2.63, dt (12.7, 7.6) β 1.79, m	38.0	2.55, m 2.25, m	37.3	2.50, m 2.07, m
16	27.1	1.55, dtd (13.1, 9.5, 5.5) 1.24, m	70.1	4.40, tt (8.0, 4.3)	216.1		214.5	
17	44.2	1.70, m	49.3	1.81, m	56.9	2.68, m	56.6	2.53, m
18	12.6	0.73, s	14.1	1.23, s	14.8	0.99, s	14.9	1.01, s
19	15.3	0.91, s	15.8	0.93, s	15.9	0.92, s	16.5	1.00, s
20	39.1	1.93, m	33.9	2.94, dtd (10.6, 6.9, 3.4)	35.7	2.47, td (7.8, 5.6)	34.8	2.36, m
21	13.0	1.00, d (6.7)	12.4	1.14, d (7.0)	13.5	1.00, d (7.1)	14.0	0.96, d (7.0)
22	78.7	4.40, dt (13.2, 3.5)	78.4	5.27, dt (13.3, 3.5)	77.8	5.13, m	77.4	4.84, ddd (12.7, 6.2, 3.4)
23	30.2	2.37, m 2.03, dd (18.1, 3.1)	30.8	2.49, dt (12.7, 7.6) 1.79, m	32.2	2.25, m	32.6	2.36, m 2.15, m
24	154.3		154.3		154.2		152.4	
25	127.9		127.9		127.9		126.1	
26	166.7		166.9		166.5		166.5	
27	56.6	4.87, d (11.7) 4.77, d (11.7)	56.7	4.75, m	56.7	4.71, m	57.5	4.34, m
28	20.5	2.11, s	20.5	2.10, s	20.5	2.00, s	20.8	2.03, s
1-OAc							20.1	2.03, s
							171.5	
2-OAc	21.4 171.0	2.17, s	21.4 171.0	2.17, s	21.4 171.0	2.15, s		
12-OAc	21.3 170.3	1.94, s	21.4 170.3	1.98, s	21.5 170.5	2.03, s	21.4 169.6	2.13, s
1-OH		5.76, d (10.0)		5.71, d (9.9)				
5-OH		7.41, s		7.32, s				3.19, s
15-OH				6.37, d (4.5)				

^a Recorded at 600 MHz (^1H) and 125 MHz (^{13}C) in pyridine-*d*₅. ^b Recorded at 500 MHz (^1H) and 125 MHz (^{13}C) in chloroform-*d*.

**Figure 6.** Key ROESY correlations for compounds 5 and 9.

Compound **6** gave protonated molecular ion peaks at m/z 641.2735 (calcd. 641.2729) in the HRESIMS, corresponding to a molecular formula of $C_{32}H_{45}O_{11}Cl$, which differed from that of **5** by one additional oxygen atom. The 1H and ^{13}C NMR spectra of **6** were highly similar to those of **5**. The only difference between these two compounds is that a methylene group in **5** was replaced by an oxygenated methine (δ_H 4.40, d, $J = 11.7$ Hz; δ_C 70.1) and a hydroxyl signal (δ_H 6.37, d, $J = 4.5$ Hz) in **6**. The 1H - 1H COSY correlations of H₂-15/H-16/H-17 and HMBC correlations (Figure S1 from Supplementary Materials) between the hydroxyl proton resonance at δ_H 6.37 and the methine carbon at δ_C 49.3 (C-17) suggested that the hydroxyl group was attached to C-16. The ROESY correlations (Figure S1 from Supplementary Materials) of H₃-19 with H-1/H-2/H₂-4 β /H-8/H₂-11 β , H-8 with H₃-18, and H₃-18 with H₂-11 β /H-12/H₂-15 β , and H₂-15 β with OH-16 indicated that they were co-facial, and β -oriented. The coupling constants of H-6 (δ_H 3.05, d, $J = 3.7$ Hz) and H-7 (δ_H 3.31, t, $J = 3.1$ Hz) indicated that the protons at C-6 and C-7 were also β -oriented. In addition, ROESY correlations of OH-1/H-3/H-9, OH-5/H₂-4 α /H-9, H-9/H-14, and H-14/H-17 showed that these protons were α -oriented. The absolute configuration of **6** was further confirmed by its ECD spectrum, which showed the similar Cotton effects to compound **5** (Figure 3). Therefore, compound **6** was defined as a 16 β -hydroxyl derivative of **5**, and named chantriolide K.

The HRESIMS and ^{13}C NMR data of chantriolide L (**7**) showed a molecular formula of $C_{32}H_{43}O_{11}Cl$, indicating a mass 2 Da less than that of **6**. The ^{13}C NMR spectrum showed one additional carbonyl signal at 216.1 ppm, suggesting the presence of one carbonyl group in **7**. The HMBC correlations (Figure S1 from Supplementary Materials) from the protons at δ_H 2.60 (H-14) and δ_H 2.47 (H-20) to the carbon at δ_C 216.1 (C-16) placed the carbonyl at C-16. The stereochemistry of **7** was established from the ROESY correlations (Figure S1 from Supplementary Materials) and the ECD spectrum (Figure 7). Compound **7** showed very similar Cotton effects to compound **2**, while both of them showed an additional negative Cotton effect around 300 nm when compared with compounds **3**, **5**, and **6**, which was obviously due to the presence of the carbonyl at C-16.

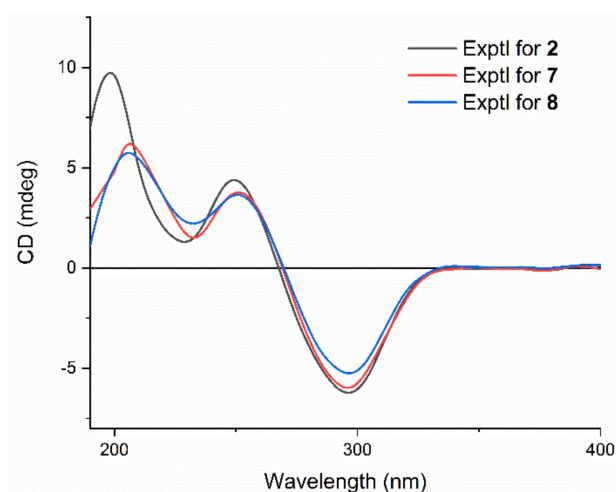


Figure 7. Experimental ECD spectra of compounds **2**, **7**, and **8**.

Compound **8** gave a molecular formula $C_{32}H_{43}O_{11}Cl$, as determined by the positive ion HRSEIMS at m/z 639.2564 [$M + H$]⁺ (calcd. for $C_{32}H_{44}ClO_{11}$, 639.2567), which was the same with that of compound **7**. The 1H NMR data of both **7** and **8** showed four methyls, two acetoxyl methyls, six oxygenated methines, and one oxygenated methylene. Compared with **7**, the chemical shifts at H-1, H-2, and H-3 in compound **8** shifted from δ_H 4.08, 5.79, and 5.10 to δ_H 5.11, 4.16, and 4.48 (Table 2), together with the HMBC correlation from the proton at δ_H 5.11 (H-1) to the carbonyl carbon at δ_C 171.5, revealed that **8** possessed an acetoxy group at C-1 and a hydroxy group at C-2. The ROESY (Figure S2 from Supplementary Materials) and ECD (Figure 7) spectra of **8** were very close to those of **7**, indicating further

that they had the same relative and absolute configuration. Consequently, the structure of compound **8** was proposed, and given a trivial name chantriolide M.

Chantriolide N (**9**), colorless crystals, was assigned a molecular formula of C₂₈H₄₄O₆ by HRESIMS and ¹³C NMR data, which is the same as that of plantagiolide M (**16**) [23]. Its 1D and 2D NMR data (Table 3, Figure 5) further established a same planar structure with **16**. The key ROESY correlations of H-1/H-3/H-9, H-9/H-7, and H-7/H-14 unveiled that the relative configurations at C-1 and C-7 in **9** changed when compared with those of compound **16**. Such elucidation was further supported by the difference of chemical shifts at H-1 (**9**: 3.83, dd, *J* = 11.9, 4.2 Hz; **16**: 3.45, dd, *J* = 11.9, 4.3 Hz) and H-7 (**9**: 4.10, d, *J* = 8.3 Hz; **16**: 3.79, dd, *J* = 5.8, 3.5 Hz). In addition, distinct proton chemical shifts were observed at 23 (**9**: 1.98, m, 1.90, m; **16**: 2.27, m, 1.79, m), 27 (**9**: 1.65, d, *J* = 7.0 Hz; **16**: 1.29, d, *J* = 7.1 Hz), and 28 (**9**: 1.56, s; **16**: 1.35, s). The absolute configuration was further confirmed by a single crystal crystallographic diffraction experiment with Cu K α radiation (CCDC 2203338, Figure 8). Accordingly, the structure of **9** was identified as a 1*R*,7*R*,24*S*,25*S*-epimer of **16**, and named chantriolide N.

Table 3. ¹H and ¹³C NMR data for compounds **9–11** (δ in ppm, *J* in Hz, in pyridine-*d*₅).

Position	9 ^a		10 ^b		11 ^a	
	δ_C	δ_H (J in Hz)	δ_C	δ_H (J in Hz)	δ_C	δ_H (J in Hz)
1	78.5	3.83, dd (11.9, 4.2)	71.0	4.54, dt (11.1, 4.7)	210.6	
2	44.2	α 2.66, m β 2.28, q (11.7)	43.5	α 2.81, dtd (12.8, 5.6, 1.6) β 2.32, q (11.6)	49.2	α 3.04, dd (13.5, 6.8) β 3.33, dd (13.5, 9.8)
3	68.4	4.01, tdd (9.6, 7.2, 4.4)	64.7	4.89, m	66.4	5.06, m
4	44.0	2.71, m	43.9	α 2.37, m β 2.14, m	43.2	2.56, m
5	141.1		72.9		73.7	
6	131.8	5.94, d (1.7)	59.4	3.14, d (3.8)	57.4	3.20, m
7	72.8	4.10, d (8.3)	57.8	3.26, dd (3.8, 2.4)	56.6	3.20, m
8	42.5	1.73, m	37.1	1.91, m	36.5	1.67, m
9	50.2	1.55, m	39.9	1.90, m	36.5	2.07, m
10	43.7		44.3		53.9	
11	24.9	α 2.96, dq (14.3, 3.7) β 1.74, m	25.0	α 2.42, m β 1.78, m	22.5	α 2.72, dq (13.0, 3.5) β 1.27, m
12	41.1	2.01, dt (14.2, 4.3) 1.29, m	41.0	1.97, m 1.13, m	40.7	1.91, m 1.14, m
13	43.7		44.0		44.2	
14	57.2	1.26, m	51.9	1.34, m	52.0	1.28, m
15	28.0	α 2.23, dt (9.3, 3.1) β 1.80, m	24.2	α 1.69, m β 1.19, m	24.1	α 1.64, m β 1.17, m
16	28.2	1.80, m 1.32, m	27.7	α 1.66, m β 1.25, m	27.7	1.64, m 1.21, m
17	52.4	1.14, m	52.6	1.06, m	52.5	0.99, m
18	12.6	0.74, s	12.5	0.67, s	12.7	0.64, s
19	14.0	1.34, s	12.1	1.17, s	16.8	1.30, s
20	40.1	2.08, ddt (9.3, 6.5, 3.1)	40.0	2.04, ddt (9.8, 7.0, 3.6)	39.9	2.01, m
21	13.6	1.06, d (6.6)	13.4	1.00, d (6.6)	13.3	0.97, d (6.6)
22	79.1	5.13, m	78.9	5.09, m	78.8	5.09, m
23	37.1	1.98, m 1.90, m	37.1	1.96, m 1.89, m	37.0	1.88, m
24	69.9		69.8		69.8	
25	47.6	2.58, q (7.0)	47.5	2.57, q (7.0)	47.5	2.56, m
26	175.1		175.0		175.0	
27	10.6	1.65, d (7.0)	10.6	1.64, d (7.0)	10.6	1.64, d (7.0)
28	28.7	1.56, s	28.6	1.56, s	28.6	1.53, s
5-OH				4.69, s		5.93, s

^a Recorded at 600 MHz (¹H) and 125 MHz (¹³C). ^b Recorded at 500 MHz (¹H) and 125 MHz (¹³C).

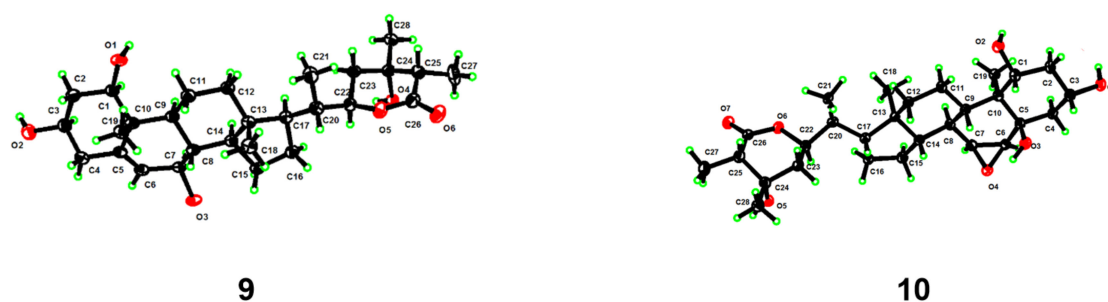
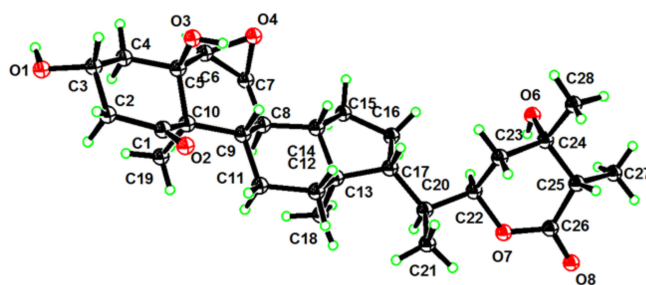


Figure 8. Perspective ORTEP drawings for compounds 9 and 10.

The molecular formula of compound **10** was determined to be $C_{28}H_{44}O_7$ by HRESIMS analysis (m/z 493.3180 $[M + H]^+$, calcd. for 493.3165), which contains one more oxygen atom than **9**. The 1H and ^{13}C NMR data (Table 3) of **10** showed characteristic signals of two epoxy methine signals [δ_H 3.26 (dd, $J = 3.8, 2.4$ Hz), 3.14 (d, $J = 3.8$ Hz); δ_C 59.4, 57.8], and one oxygenated quaternary carbon signal (δ_C 72.9). The location of this epoxy group at C-6 and C-7 was deduced by the 1H - 1H COSY correlations of H-6/H-7/H-8. Furthermore, the C-5 was designated as an oxygenated quaternary carbon by the HMBC correlations (Figure S1 from Supplementary Materials) from the hydroxyl proton at 4.69 ppm (5-OH) to C-4 (δ_C 43.9), C-5 (δ_C 72.9), and C-6 (δ_C 59.4). The whole structure was confirmed through a single crystal crystallographic diffraction experiment with Cu $K\alpha$ radiation (CCDC 2203339, Figure 8). A trivial name chantriolide O was given to **10**, and its structure is shown in Figure 1.

Chantriolide P (**11**) was obtained as colorless crystals and assigned a molecular formula of $C_{28}H_{42}O_7$ from its HRESIMS and ^{13}C NMR data, corresponding to eight indices of hydrogen deficiency. Its molecular weight was 2 Da less than that of chantriolide O (**10**). Its carbon NMR data (Table 3), when compared with that of **10**, showed the presence of one additional ketone group (δ_C 210.6), which was designated as C-1 by the HMBC correlation (Figure S1 from Supplementary Materials) from Me-19 at δ_H 1.30 and H₂-2 at δ_H 3.33, 3.04 to this carbon. The relative configuration was deduced by the ROESY correlations, and the whole structure was further confirmed by a single crystal crystallographic diffraction experiment with Cu $K\alpha$ radiation (CCDC 2203341, Figure 9). Subsequently, the structure of compound **11** was established, and named chantriolide P.



11

Figure 9. Perspective ORTEP drawings for compound 11.

Apart from compounds 1–11, six other known compounds were isolated and identified as plantagiolide E (**12**) [21], plantagiolide C (**13**) [21], plantagiolide B (**14**) [21], plantagiolide A (**15**) [21], plantagiolide M (**16**) [23], and chantriolide D (**17**) [24] by comparing their spectroscopic data with those reported in literature.

2.2. Hepatoprotective Effect Assay

The rhizomes of *T. chantrieri* have been used for the treatment of hepatitis [33]. Several withanolides were reported to protect hepatocytes against oxidative injury in H₂O₂-treated LO2 [34] or AML12 cells [35]. Herein, the hepatoprotective effect of all the isolates were evaluated on *t*-BHP-injured AML12 hepatocytes. Firstly, the noncytotoxic concentrations of compounds 1–17 on AML12 hepatocytes were evaluated by the MTT [3-(4,5-dimethylthiazol-2-yl)-2,5-diphenyltetrazolium bromide] assay. The MTT results showed that compounds 1–7, 9, 10, 12, 13, 15, and 17 did not show evident cytotoxicity up to 40 μ M, while the maximum safe concentrations of compounds 11, 14, and 16 were 20 μ M, and that of compound 8 was 10 μ M (Figure S103 from Supplementary Materials). *t*-BHP at 100 μ M significantly decreased the viability of AML12 hepatocytes ($p < 0.01$); whereas, compounds 5–11 and 16 at their maximum safe concentration obviously increased cell viability compared to the *t*-BHP group, and resveratrol (Res) at 10 μ M was used as a positive control (Figure 10A). Furthermore, compound 8 dose-dependently increased the viability of *t*-BHP-injured AML12 hepatocytes (Figure 10B). *t*-BHP treatment observably increased reactive oxygen species (ROS) accumulation and decreased glutathione (GSH) level, while compound 8 dose-dependently reversed the changes (Figure 10C,D). The above results indicated that compound 8 protected AML12 hepatocytes against *t*-BHP injury by decreasing ROS accumulation and increasing the GSH level.

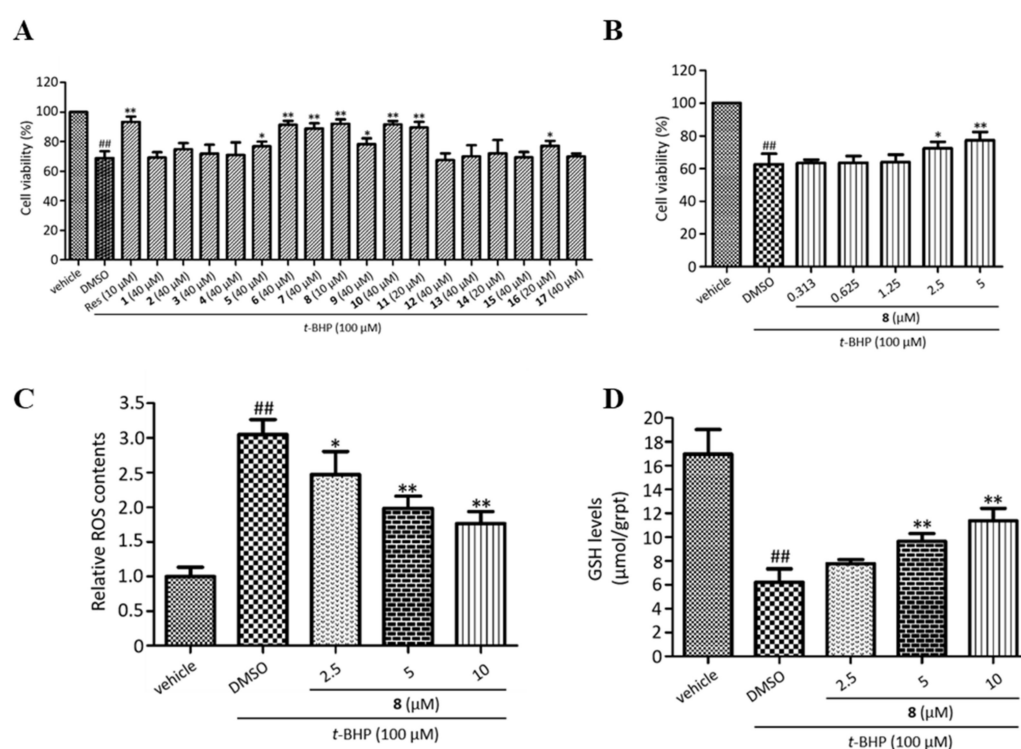


Figure 10. Hepatoprotective effects of withanolides on *t*-BHP-injured AML12 hepatocytes. (A) Cell viability of *t*-BHP-injured AML12 hepatocytes treated with compounds 1–17 at their maximum safe concentration. Resveratrol (Res) at 10 μ M was used as a positive control. (B) Cell viability of *t*-BHP-injured AML12 hepatocytes treated with different concentrations of compound 8. (C) ROS contents in *t*-BHP-injured AML12 hepatocytes treated with different concentrations of compound 8. (D) GSH levels in *t*-BHP-injured AML12 hepatocytes treated with different concentrations of compound 8. Data are shown as mean \pm S.D., $n = 3$. ## $p < 0.01$ vs. vehicle; * $p < 0.05$ and ** $p < 0.01$ vs. *t*-BHP plus DMSO.

The nuclear factor erythroid 2-related factor 2 (Nrf2), is the main regulator of the oxidative stress response [36,37]. Under homeostatic conditions, Nrf2 is kept inactive being bound to its endogenous inhibitor, Kelch-like ECH-associated protein 1 (Keap-1) [38].

Under oxidative stress, Nrf2 detaches from Keap-1 and translocates to the nucleus, inducing the expression of antioxidant genes [39]. Heme oxygenase-1 (HO-1) acts as an important antioxidant enzyme to maintain redox homeostasis [40]. Herein, compound **8** at 2.5, 5, and 10 μM decreased the protein expression of Keap-1, and increased the protein expression of Nrf2 and HO-1 in *t*-BHP-injured AML12 hepatocytes (Figure 11A). Furthermore, compound **8** increased the nuclear translocation of Nrf2 assessed by immunofluorescent images and Western blotting (Figure 11B,C). Thus, compound **8** decreased ROS accumulation and increased GSH level by regulating the Keap-1/Nrf2/HO-1 pathway in *t*-BHP-injured AML12 hepatocytes.

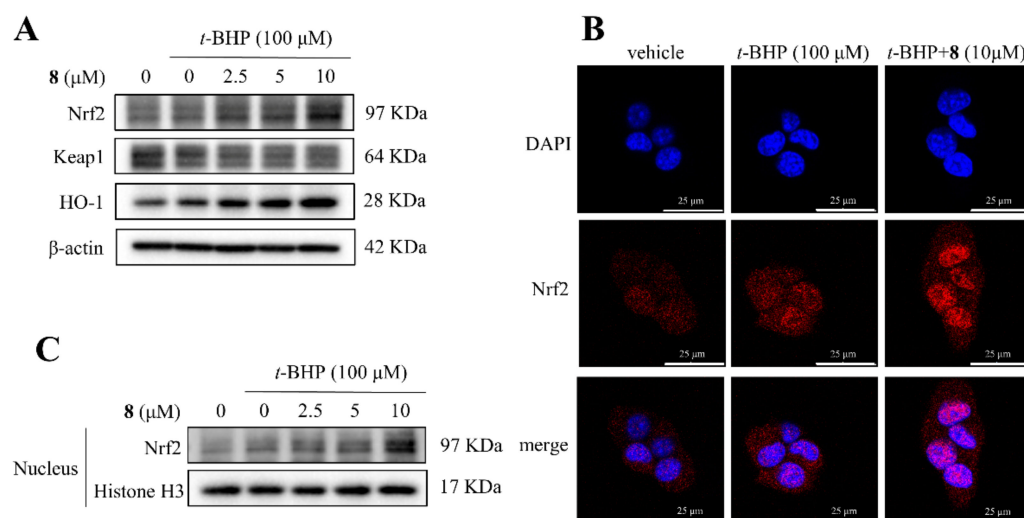


Figure 11. Compound **8** activates Keap-1/Nrf2/HO-1 signaling pathway in *t*-BHP-injured AML12 hepatocytes. (A) The total protein levels of Keap-1, Nrf2, and HO-1 were analyzed by Western blots. β -actin was used as a loading control. (B) Representative immunofluorescent image of Nrf2 distribution. Nuclei were visualized using DAPI (blue), and Nrf2 was stained as red. Scale bar = 25 μm . (C) Nuclear Nrf2 expression was analyzed by Western blots. Histone H3 was used as a loading control.

In summary, a phytochemical investigation of *T. chantrieri* led to the isolation of 17 withanolides, including 11 new derivatives. Most of them contain an acetoxy or hydroxyl group attached to C-1 and the epoxy moiety at C-3/C-4 or C-6/C-7. Compounds **5–8** have rare substitutions of chlorine atoms, which are unusual for withanolide-type natural products. The absolute configuration for the new withanolides was confirmed by single X-ray diffraction crystallography and electronic circular dichroism analysis. The isolates were evaluated for their hepatoprotective activity on *t*-BHP-injured AML12 hepatocytes. Compounds **5–11** and **16** significantly increased viability of *t*-BHP-injured cells. Additionally, compound **8**, the representative withanolide with the best hepatoprotective activity, was proved to decrease ROS accumulation and increase GSH level by regulating the Keap-1/Nrf2/HO-1 pathway in *t*-BHP-injured AML12 hepatocytes.

3. Materials and Methods

3.1. General Experimental Procedures

Rudolph Research Analytical Autopol VI automatic polarimeter was used to optical rotations values. IR spectra were acquired on a Nicolet Magna FRIR-750 spectrometer. ECD spectra were obtained on a JASCO J-810 spectrometer. HRESIMS data were recorded on the Waters Synapt G2-Si Q-ToF and Agilent G6520 Q-ToF mass spectrometers. 1D and 2D NMR spectra were recorded using a BrukerAvance III-500 (600) spectrometer and a Varian MR-400 spectrometer. The chemical shift (δ) values are given in ppm with coupling constants (J) in hertz, and the residual signals of Pyridine and CHCl_3 were used as internal standards. Single-crystal X-ray diffraction measurements were conducted on a Bruker D8 Venture diffractometer or a Bruker Apex-II CCD diffractometer. LCESIMS data were recorded on a

Waters 2695 instrument with a 2998 PDA detector equipped with a Waters Acquity ELSD, and a Waters 3100 SQDMS detector. Preparative HPLC was performed on a Varian PrepStar system with an Alltech 3300 ELSD with a Waters Sunfire RP C₁₈, 5 μm, 30 × 150 mm column. MCI gel CHP20P (75–150 μm, Mitsubishi Chemical Industries, Tokyo, Japan), silica gel (100–200, 200–300, and 300–400 mesh, Qingdao Marine Chemical Industrials, Qingdao, China), ODS gel AAG12S50 (12 nm, S-50 μm, YMC, Japan) and Sephadex LH-20 (Pharmacia Biotech AB, Uppsala, Sweden) was used for column chromatography. TLC was performed on pre-coated silica gel GF254 plates (Yantai Chemical Industrials, Yantai, China), and the TLC spots were visualized with 5% H₂SO₄ in EtOH containing 10 mg/mL vanillin, followed by heating.

3.2. Plant Material

The rhizomes of *T. chantrieri* were collected from Jinghong City, Xishuangbanna Dai Autonomous Prefecture, Yunnan Province, China, in October 2016, and identified by one of the authors (Xiao-Rong Wang). A voucher specimen (no. 20161006) was deposited in the Herbarium of the Shanghai Institute of Materia Medica, Chinese Academy of Sciences.

3.3. Extraction and Isolation

The air-dried and ground rhizomes of *T. chantrieri* (15 kg) were extracted with 95% EtOH (4 × 40 L, 3 days each) at room temperature. The percolates were combined and evaporated under pressure to afford a crude extract (1.4 kg), which was then suspended in water and partitioned successively with petroleum ether, EtOAc, and *n*-BuOH. The EtOAc fraction (90 g) was separated with MCI column (EtOH/H₂O, from 30 to 95%, and finally acetone), yielding five fractions (Fr. 1–Fr. 5). Fr. 2 was then treated with a silica gel column (200–300 mesh) eluted with a mixture of CH₂Cl₂/acetone (20:1, 15:1, 10:1, 8:1, 6:1, 5:1, 2:1) to give Fr. 2A–2M. Fr. 2I was separated on Sephadex LH-20 (eluted with MeOH) to afford 2I1–2I6. Fr. 2I3 was further purified by Sephadex LH-20 gel (eluted with MeOH) to give subfractions 2I3A–2I3D. Fr. 2I3B was subjected to a silica gel (300–400 mesh) column chromatography using a gradient solvent system of CH₂Cl₂/MeOH (80:1, 60:1, 50:1, 20:1, 5:1) to give seven subfractions (2I3B1–2I3B7). Compound **2** (15 mg, *t*_R = 13.07 min) was isolated from Fr. 2I3B2 by preparative HPLC (MeCN/H₂O: 0–120 min, from 22 to 52%). Subfractions Fr. 2J1–Fr. 2J5 were obtained from Fr. 2J via using a Sephadex LH-20 column (eluted with MeOH). Fr. 2J1 was separated by CC over ODS gel (MeOH/H₂O: from 40 to 70%, and 100%) to yield subfractions 2J1A–Fr. 2J1D. Fr. 2J1A was subjected to preparative HPLC using MeCN/H₂O as the mobile phase (0–120 min, from 15 to 45%), to afford compound **12** (79 mg, *t*_R = 11.02 min). Compounds **1** (30 mg, *t*_R = 11.22 min) and **13** (336 mg, *t*_R = 11.52 min) were obtained from Fr. 2J1B by preparative HPLC (MeCN/H₂O: 0–120 min, from 16 to 46%). Fr. 2J2A–Fr. 2J2K were obtained from Fr. 2J2 by CC over ODS gel (MeOH/H₂O: from 40 to 60%, and 100%). Fr. 2J2F was further purified by preparative HPLC (MeCN/H₂O: 0–120 min, from 18 to 48%) to give compound **11** (3 mg, *t*_R = 12.08 min). Fr. 2K was separated by column chromatography (CC) over Sephadex LH-20 (eluted with MeOH) to afford subfractions 2K1–2K7. Then, Fr. 2K1 and Fr. 2K2 were separated by a silica gel column (200–300 mesh, CH₂Cl₂/acetone) to give 2K1A–2K1K. Fr. 2K1E was treated with an ODS column (MeOH/H₂O: from 35 to 75%, and 100%) and then purified by preparative HPLC using MeCN/H₂O (0–120 min, from 18 to 48%) to afford compounds **7** (42 mg, *t*_R = 12.57 min), **8** (4 mg, *t*_R = 10.17 min), and **17** (10 mg, *t*_R = 11.98 min). Fr. 2K1F was subjected to the preparative HPLC using MeCN/H₂O (0–120 min, from 11 to 41%) to yield compound **15** (86 mg, *t*_R = 10.03 min). Fr. 2K1G was separated by a Sephadex LH-20 column (eluted with MeOH) and then purified by an ODS column eluted with a gradient of aqueous MeOH (from 40 to 80%, and 100%), affording six fractions (2K1G1A–2K1G1F). Compounds **3** (7 mg, *t*_R = 10.68 min) and **10** (4 mg, *t*_R = 10.25 min) were isolated from Fr. 2K1G1A and Fr. 2K1G1B by preparative HPLC (MeCN/H₂O: 0–120 min, from 16 to 36% and 18 to 48%, respectively). Fr. 2K1G1B5 was further purified with preparative TLC (CH₂Cl₂/MeOH = 14:1) to yield compound **6** (31 mg, *t*_R = 10.02 min). Fr. 2K1H was subjected to an ODS

column (MeOH/H₂O: from 30 to 65%, and 100%) to give subfractions 2K1H1–2K1H11. Fr. 2K1H3 and Fr. 2K1H5 were purified by preparative HPLC (MeCN/H₂O: 0–120 min, from 10 to 40%, and 12 to 42%, respectively) to afford compounds **4** (18 mg, *t*_R = 10.33 min) and **14** (261 mg, *t*_R = 9.63 min). Subfractions 2L1–2L8 were yielded from Fr. 2L by using an ODS gel column eluted with aqueous MeOH (from 35 to 80%, and 100%). Fr. 2L5 was subjected to the preparative HPLC using MeCN/H₂O (0–120 min, from 15 to 45%) to give Fr. 2L5A. Compounds **9** (25 mg, *t*_R = 10.52 min) and **16** (24 mg, *t*_R = 11.02 min) were obtained from Fr. 2L5A by a silica gel column (CH₂Cl₂/MeOH = 15:1). Fr. 3 was separated on a Sephadex LH-20 (eluted with CHCl₃/MeOH 1:1), yielding Fr. 3A–3G. Fr. 3B was subsequently treated with an ODS column eluted with aqueous MeOH (from 45 to 80%, and 100%) to give fractions Fr. 3B1–3B11. Subfractions Fr. 3B5A–5I were yielded from Fr. 3B5 by using a silica gel column eluted with a mixture of CH₂Cl₂/MeOH (80:1, 60:1, 30:1, 15:1, 5:1). Fr. 3B5E was purified with preparative HPLC using MeCN/H₂O (0–120 min, from 35 to 55%) to afford compound **5** (2 mg, *t*_R = 14.52 min).

Chantriolide F (**1**): Colorless crystals (acetonitrile); mp 296–297 °C; [α]_D²⁰ + 72 (*c* 1.3, MeOH); IR (KBr) ν_{\max} 3480, 2920, 1732, 1605, 1383, 1249, 1136, 1028 cm⁻¹; ¹H and ¹³C NMR, see Table 1; HRESIMS *m/z* 651.3023 [M + HCOO]⁻ (calcd. for C₃₃H₄₇O₁₃, 651.3017).

Chantriolide G (**2**): Colorless crystals (acetonitrile); mp 289–290 °C; [α]_D²⁰ + 16 (*c* 0.8, MeOH); UV (MeOH) λ_{\max} (log ϵ) 204 (2.64), 223 (2.63); IR (KBr) ν_{\max} 3492, 2956, 2921, 2851, 1735, 1701, 1462, 1378, 1244, 1028 cm⁻¹; ¹H and ¹³C NMR, see Table 1; HRESIMS *m/z* 587.2865 [M + H]⁺ (calcd. for C₃₂H₄₃O₁₀, 587.2856).

Chantriolide H (**3**): White powder; [α]_D²⁰ + 53 (*c* 1.4, MeOH); UV (MeOH) λ_{\max} (log ϵ) 203 (2.49); IR (KBr) ν_{\max} 3474, 2955, 2925, 1737, 1704, 1380, 1247, 1027 cm⁻¹; ¹H and ¹³C NMR, see Table 1; HRESIMS *m/z* 547.2914 [M + H]⁺ (calcd. for C₃₀H₄₃O₉, 547.2907).

Chantriolide I (**4**): Colorless crystals (acetonitrile); mp 247–248 °C; [α]_D²⁰ + 46 (*c* 1.3, MeOH); IR (KBr) ν_{\max} 3470, 2958, 2924, 1737, 1379, 1258, 1029 cm⁻¹; ¹H and ¹³C NMR, see Table 1; HRESIMS *m/z* 622.3237 [M + NH₄]⁺ (calcd. for C₃₂H₄₈NO₁₁, 622.3227).

Chantriolide J (**5**): Colorless crystals (acetonitrile); mp > 260 °C; [α]_D²⁰ - 6 (*c* 0.9, MeOH); UV (MeOH) λ_{\max} (log ϵ) 203 (2.77); IR (KBr) ν_{\max} 3445, 2965, 2925, 1738, 1382, 1246, 1026, 736 cm⁻¹; ¹H and ¹³C NMR, see Table 2; HRESIMS *m/z* 669.2689 [M + HCOO]⁻ (calcd. for C₃₃H₄₆ClO₁₂, 669.2678).

Chantriolide K (**6**): White powder; [α]_D²⁰ + 21 (*c* 1.1, MeOH); UV (MeOH) λ_{\max} (log ϵ) 214 (2.59); IR (KBr) ν_{\max} 3449, 2955, 2924, 1732, 1714, 1698, 1382, 1244, 1028 cm⁻¹; ¹H and ¹³C NMR, see Table 2; HRESIMS *m/z* 641.2735 [M + H]⁺ (calcd. for C₃₂H₄₆ClO₁₁, 641.2729).

Chantriolide L (**7**): White powder; [α]_D²⁰ - 66 (*c* 1.2, MeOH); UV (MeOH) λ_{\max} (log ϵ) 200 (2.61); IR (KBr) ν_{\max} 3466, 2958, 2925, 1733, 1382, 1244, 1029 cm⁻¹; ¹H and ¹³C NMR, see Table 2; HRESIMS *m/z* 639.2570 [M + H]⁺ (calcd. for C₃₂H₄₄ClO₁₁, 639.2567).

Chantriolide M (**8**): White powder; [α]_D²⁰ - 78 (*c* 0.9, MeOH); UV (MeOH) λ_{\max} (log ϵ) 202 (2.74); IR (KBr) ν_{\max} 3445, 2957, 2924, 1738, 1715, 1394, 1384, 1244, 1041 cm⁻¹; ¹H and ¹³C NMR, see Table 2; HRESIMS *m/z* 639.2564 [M + H]⁺ (calcd. for C₃₂H₄₄ClO₁₁, 639.2567).

Chantriolide N (**9**): Colorless crystals (acetonitrile); mp 262–263 °C; [α]_D²⁰ + 20 (*c* 1.2, MeOH); IR (KBr) ν_{\max} 3406, 2960, 2921, 2847, 1467, 1384, 1068, 1019 cm⁻¹; ¹H and ¹³C NMR, see Table 3; HRESIMS *m/z* 499.3026 [M + Na]⁺ (calcd. for C₂₈H₄₄O₆Na, 499.3036).

Chantriolide O (**10**): Colorless crystals (acetonitrile); mp 227–229 °C; [α]_D²⁰ - 18 (*c* 1.3, MeOH); IR (KBr) ν_{\max} 3462, 2956, 2923, 2869, 1463, 1456, 1372, 1260, 1079, 1015 cm⁻¹; ¹H and ¹³C NMR, see Table 3; HRESIMS *m/z* 493.3180 [M + H]⁺ (calcd. for C₂₈H₄₅O₇, 493.3165).

Chantriolide P (**11**): Colorless crystals (acetonitrile); mp 279–281 °C; [α]_D²⁰ + 53 (*c* 1.5, MeOH); IR (KBr) ν_{\max} 3466, 2955, 2925, 2870, 2853, 1713, 1699, 1462, 1456, 1379, 1098 cm⁻¹; ¹H and ¹³C NMR, see Table 3; HRESIMS *m/z* 508.3284 [M + NH₄]⁺ (calcd. for C₂₈H₄₆NO₇, 508.3274).

3.4. X-ray Crystallographic Analysis of Compounds 1, 2, 4, 5, 9, 10, and 11

The crystals were obtained from their MeCN solutions, and suitable crystals were selected for X-ray crystallographic analysis. The structures were settled and refined by using the Bruker SHELXTL Software Package. Copies of crystallographic data of every crystal can be obtained free of charge via the internet at www.ccdc.cam.ac.uk/conts/retrieving.html or on application to CCDC, 12 Union Road, Cambridge CB2 1EZ, UK [Tel.: (+44)-1223-336-408; Fax: (+44)-1223-336-033; E-mail: deposit@ccdc.cam.ac.uk].

Crystal data for Compound 1. The crystal was kept at 170 K during data collection. $C_{32}H_{46}O_{11}$: $M = 606.69$ g/mol, orthorhombic, space group $P2_12_12_1$ (no. 19), $a = 9.3329(6)$ Å, $b = 11.1622(7)$ Å, $c = 29.548(2)$ Å, $\alpha = 90^\circ$, $\beta = 90^\circ$, $\gamma = 90^\circ$, $V = 3078.2(3)$ Å³, $Z = 4$, $T = 170$ K, $\mu(\text{Cu K}\alpha) = 0.812$ mm⁻¹, $F = 1304.0$, $D_{\text{calc}} = 1.309$ g/cm³, 42,286 reflections measured ($5.982^\circ \leq 2\sigma \leq 149.77^\circ$), 6295 unique ($R_{\text{int}} = 0.0470$, $R_{\text{sigma}} = 0.0295$), which were used in all calculations. The final R_1 was 0.0437 ($I > 2\sigma(I)$) and wR_2 was 0.1218. Flack parameter: 0.05(4). Crystallographic data for 1 were deposited at the Cambridge Crystallographic Data Centre as deposit no. CCDC 2203317.

Crystal data for Compound 2. The crystal was kept at 220 K during data collection. $C_{32}H_{42}O_{10}$: $M = 586.65$ g/mol, orthorhombic, space group $P2_12_12_1$ (no. 19), $a = 11.1641(4)$ Å, $b = 9.3279(3)$ Å, $c = 28.8901(12)$ Å, $\alpha = 90^\circ$, $\beta = 90^\circ$, $\gamma = 90^\circ$, $V = 3008.55(19)$ Å³, $Z = 4$, $T = 220$ K, $\mu(\text{Cu K}\alpha) = 0.790$ mm⁻¹, $F = 1256.0$, $D_{\text{calc}} = 1.295$ g/cm³, 30,900 reflections measured ($6.118^\circ \leq 2\sigma \leq 133.192^\circ$), 5130 unique ($R_{\text{int}} = 0.0850$, $R_{\text{sigma}} = 0.0555$), which were used in all calculations. The final R_1 was 0.0469 ($I > 2\sigma(I)$) and wR_2 was 0.1239. Flack parameter: $-0.03(13)$. Crystallographic data for 2 were deposited at the Cambridge Crystallographic Data Centre as deposit no. CCDC 2203323.

Crystal data for Compound 4. The crystal was kept at 170 K during data collection. $C_{34}H_{49}NO_{12}$: $M = 663.74$ g/mol, orthorhombic, space group $P2_12_12_1$ (no. 19), $a = 9.0286(2)$ Å, $b = 12.9608(3)$ Å, $c = 27.8297(6)$ Å, $\alpha = 90^\circ$, $\beta = 90^\circ$, $\gamma = 90^\circ$, $V = 3256.57(13)$ Å³, $Z = 4$, $T = 170$ K, $\mu(\text{Cu K}\alpha) = 0.849$ mm⁻¹, $F = 1424.0$, $D_{\text{calc}} = 1.354$ g/cm³, 25,652 reflections measured ($6.352^\circ \leq 2\sigma \leq 149.212^\circ$), 6332 unique ($R_{\text{int}} = 0.0392$, $R_{\text{sigma}} = 0.0322$), which were used in all calculations. The final R_1 was 0.0363 ($I > 2\sigma(I)$) and wR_2 was 0.1051. Flack parameter: 0.06(6). Crystallographic data for 4 were deposited at the Cambridge Crystallographic Data Centre as deposit no. CCDC 2203333.

Crystal data for Compound 5. The crystal was kept at 140 K during data collection. $C_{32}H_{47}ClO_{11}$: $M = 643.14$ g/mol, monoclinic, space group $P2_1$ (no. 4), $a = 7.5473(5)$ Å, $b = 13.8320(9)$ Å, $c = 15.5074(10)$ Å, $\alpha = 90^\circ$, $\beta = 92.590(5)^\circ$, $\gamma = 90^\circ$, $V = 1617.23(18)$ Å³, $Z = 2$, $T = 140$ K, $\mu(\text{Cu K}\alpha) = 1.545$ mm⁻¹, $F = 688.0$, $D_{\text{calc}} = 1.321$ g/cm³, 9921 reflections measured ($5.704^\circ \leq 2\sigma \leq 127.678^\circ$), 4748 unique ($R_{\text{int}} = 0.0635$, $R_{\text{sigma}} = 0.0889$), which were used in all calculations. The final R_1 was 0.0725 ($I > 2\sigma(I)$) and wR_2 was 0.2176. Flack parameter: 0.12(2). Crystallographic data for 5 were deposited at the Cambridge Crystallographic Data Centre as deposit no. CCDC 2203335.

Crystal data for Compound 9. The crystal was kept at 150 K during data collection. $C_{60}H_{96}N_2O_{13}$: $M = 1053.38$ g/mol, monoclinic, space group $C2$ (no. 5), $a = 31.1775(11)$ Å, $b = 10.9614(4)$ Å, $c = 21.7690(7)$ Å, $\alpha = 90^\circ$, $\beta = 129.3350(10)^\circ$, $\gamma = 90^\circ$, $V = 5754.1(4)$ Å³, $Z = 4$, $T = 150$ K, $\mu(\text{Cu K}\alpha) = 0.678$ mm⁻¹, $F = 2296.0$, $D_{\text{calc}} = 1.216$ g/cm³, 40,634 reflections measured ($5.248^\circ \leq 2\sigma \leq 149.634^\circ$), 11,598 unique ($R_{\text{int}} = 0.0410$, $R_{\text{sigma}} = 0.0375$), which were used in all calculations. The final R_1 was 0.0498 ($I > 2\sigma(I)$) and wR_2 was 0.1418. Flack parameter: 0.01(4). Crystallographic data for 9 were deposited at the Cambridge Crystallographic Data Centre as deposit no. CCDC 2203338.

Crystal data for Compound 10. The crystal was kept at 170 K during data collection. $C_{28}H_{54}O_{12}$: $M = 582.71$ g/mol, monoclinic, space group $P2_1$ (no. 4), $a = 14.1483(13)$ Å, $b = 5.9754(5)$ Å, $c = 19.3151(16)$ Å, $\alpha = 90^\circ$, $\beta = 109.720(5)^\circ$, $\gamma = 90^\circ$, $V = 1537.2(2)$ Å³, $Z = 2$, $T = 170$ K, $\mu(\text{Cu K}\alpha) = 0.807$ mm⁻¹, $F = 636.0$, $D_{\text{calc}} = 1.259$ g/cm³, 23,412 reflections measured ($4.86^\circ \leq 2\sigma \leq 149.72^\circ$), 6167 unique ($R_{\text{int}} = 0.0823$, $R_{\text{sigma}} = 0.0794$), which were used in all calculations. The final R_1 was 0.0761 ($I > 2\sigma(I)$) and wR_2 was 0.2051.

Flack parameter: 0.05(15). Crystallographic data for **10** were deposited at the Cambridge Crystallographic Data Centre as deposit no. CCDC 2203339.

Crystal data for Compound 11. The crystal was kept at 220 K during data collection. $C_{28}H_{44}O_8$: $M = 508.63$ g/mol, monoclinic, space group P21 (no. 4), $a = 13.7016(5)$ Å, $b = 6.5627(2)$ Å, $c = 14.6317(5)$ Å, $\alpha = 90^\circ$, $\beta = 90.629(2)^\circ$, $\gamma = 90^\circ$, $V = 1315.60(8)$ Å³, $Z = 2$, $T = 220$ K, $\mu(\text{Cu K}\alpha) = 0.757$ mm⁻¹, $F = 552.0$, $D_{\text{calc}} = 1.284$ g/cm³, 19,688 reflections measured ($6.04^\circ \leq 2\sigma \leq 141.098^\circ$), 4713 unique ($R_{\text{int}} = 0.0448$, $R_{\text{sigma}} = 0.0355$), which were used in all calculations. The final R_1 was 0.0360 ($I > 2\sigma(I)$) and wR_2 was 0.1041. Flack parameter: $-0.06(12)$. Crystallographic data for **11** were deposited at the Cambridge Crystallographic Data Centre as deposit no. CCDC 2203341.

3.5. Cell Culture

The murine hepatic AML12 cells were purchased from American Type Culture Collection (Rockville, MD, USA) and cultured in DMEM supplemented with 10% fetal bovine serum (Thermo, Rockford, IL, USA), 5 mg/mL insulin, 5 mg/L transferrin, and 5 µg/L selenous acid (Peiyuan, Shanghai, China) in a humidified incubator containing 5% CO₂ at 37 °C [41].

3.6. Cell Viability

The cell viability was evaluated by a colorimetric MTT method as described in our previous report [41]. AML12 cells (1×10^4 cells/well) were seeded into 96-well plates and cultured for 24 h. Then, the cells were treated with *t*-BHP (100 µM) and with or without compounds **1–17** at different concentrations for 12 h. Then, medium with 1 mg/mL MTT was added into each well. After incubating for 4 h, 150 µL DMSO was added to solubilize formazan precipitates. Finally, the absorptions at 570 nm were measured using a microplate reader (FlexStation 3, Molecular Devices, CA, USA). DMSO was used as a blank control, and resveratrol (Res) at 10 µM was used as a positive control.

3.7. Intracellular ROS Determination

Intracellular ROS levels were detected using 2,7-dichlorodihydrofluorescein diacetate (DCFH-DA, Invitrogen, Carlsbad, CA, USA) as previously described [42]. In brief, AML12 cells (1×10^4 cells/well) were seeded into each well of 96-well plates and cultured for 24 h. The cells were treated with *t*-BHP (100 µM) and different concentrations of compound **8** (0, 2.5, 5, and 10 µM) for 12 h, and then incubated with DCFH-DA (10 µM) at 37 °C in the dark for 20 min. The fluorescence intensity was measured using the microplate reader with excitation and emission wavelength at 488 and 525 nm, respectively.

3.8. Determination of GSH Level

The AML12 cells were treated with *t*-BHP (100 µM) and different concentrations of compound **8** (0, 2.5, 5, and 10 µM) for 12 h. The levels of GSH were determined using a commercial assay kit (Nanjing Jiancheng, Nanjing, Jiangsu, China) in accordance with the manufacturer's protocols. Protein concentration was determined by a BCA Protein Assay Kit (Pierce, Rockford, IL, USA). GSH levels were normalized by total protein content.

3.9. Western Blot Analysis

The AML12 cells were treated with *t*-BHP (100 µM) and different concentrations of compound **8** (0, 2.5, 5, and 10 µM) for 12 h. After washed in pre-cooling PBS, the cells were lysed in RIPA buffer (Beyotime, Shanghai, China) containing EDTA and protein phosphatase inhibitors. Equal amounts of protein (20 µg) were separated via SDS-PAGE and transferred onto PVDF membranes, where they were stained with antibodies specific to the target proteins [anti-β-actin, anti-Keap-1, anti-Nrf2, and anti-HO-1 (Cell Signaling, Danvers, MA, USA)] overnight after being blocked for 2 h in TBST containing 5% non-fat dried milk. Then, the membranes were probed with an HRP-conjugated secondary

antibody for 1 h at room temperature after washed using TBST. The bands were visualized using the ChemiDoc MP Imaging System (Bio-Rad, Hercules, CA, USA).

3.10. Confocal Immunofluorescence

AML12 cells were treated with *t*-BHP (100 μ M) and with or without compound **8** (10 μ M) for 12 h. The cells were blocked with 5% BSA after fixed with 4% paraformaldehyde. Then, the specific primary antibody (1:100 dilution) was added and incubated at 4 °C overnight and then washed twice with 0.1% triton buffer, followed by incubating with the Texas Red-conjugated secondary antibody (1:1000 dilution, Invitrogen) for 2 h at room temperature. The fluorescent images were captured by a confocal microscope (Olympus, Tokyo, Japan).

3.11. Nucleus Isolation

Nuclear proteins were extracted from AML12 cells using a Nuclear Protein Extract Kit (Beyotime). In brief, the AML12 cells were treated with *t*-BHP (100 μ M) and different concentrations of compound **8** (0, 2.5, 5, and 10 μ M) for 12 h. The cells were re-suspended in 200 μ L buffer A and then vortexed for 5 s. After incubation on ice for 15 min, 10 μ L buffer B was added and then vortexed for 5 s. The supernatant was discarded after centrifugation at 16,000 \times *g* for 5 min at 4 °C. The pellet was re-suspended in 50 μ L nuclear extraction buffer and then vortexed for 30 s. The nuclei proteins were collected in the supernatant by centrifugation at 16,000 \times *g* for 5 min at 4 °C.

3.12. Statistical Analysis

All experiments were performed with at least three biological replicates. Data are presented as the mean \pm standard deviation (S.D.) and the significant differences among multiple groups were analyzed with one-way ANOVA, followed by Tukey's post-hoc test. Figures were prepared using GraphPad Prism software Version 7.0 (GraphPad Software, Inc., San Diego, CA, USA). The analyses were conducted considering $p < 0.05$ as a significant difference in all comparisons.

Supplementary Materials: The following supporting information can be downloaded at: <https://www.mdpi.com/article/10.3390/molecules27238197/s1>, Key ^1H - ^1H COSY and HMBC correlations of compounds **1–4**, **6–8**, **10**, and **11**; key NOESY correlations of compounds **1–3**; key ROESY correlations of compounds **4**, **6–8**, **10**, and **11**; 1D and 2D NMR data, IR spectra, and HRESIMS spectra of new compounds (**1–11**); 1D NMR of known compounds (**12–17**); Cytotoxicity of compounds **1–17** on AML-12 hepatocytes; X-ray crystallographic data (CIFs) for compounds **1**, **2**, **4**, **5**, **9**, **10**, and **11**.

Author Contributions: Conceptualization, C.T. and Y.Y. (Yang Ye); Funding acquisition, S.Y., L.L. and Y.Y. (Yang Ye); Investigation, Y.Y. (Yue Yang), F.Z., M.W. and M.T.; Methodology, C.K.; Project administration, S.Y.; Resources, X.-R.W.; Software, Y.Y. (Yue Yang); Supervision, L.L. and Y.Y. (Yang Ye); Validation, C.K., L.L. and C.T.; Writing—original draft, Y.Y. (Yue Yang) and F.Z.; Writing—review and editing, C.T. All authors have read and agreed to the published version of the manuscript.

Funding: This research was funded by the National Science and Technology Major Project (Grant No. 2019ZX09201004-003-042), the National Natural Science Foundation of China (Grant Nos. 21920102003, 81903485, 81872754), the Research Fund of University of Macau (Grant No. MYRG2020-00091-ICMS), and the Internal Research Grant of the State Key Laboratory of Quality Research in Chinese Medicine, University of Macau (Grant No. QRCM-IRG2022-014).

Institutional Review Board Statement: Not applicable.

Informed Consent Statement: Not applicable.

Data Availability Statement: All data generated or analyzed during this study are included in this published article.

Conflicts of Interest: The authors declare no conflict of interest.

Sample Availability: Samples of compounds **1–17** are available from the authors.

References

1. Tomita, T.; Wadhwa, R.; Kaul, S.C.; Kurita, R.; Kojima, N.; Onishi, Y. Withanolide Derivative 2,3-Dihydro-3 β -methoxy Withaferin-A Modulates the Circadian Clock via Interaction with RAR-Related Orphan Receptor α (ROR α). *J. Nat. Prod.* **2021**, *84*, 1882–1888. [[CrossRef](#)] [[PubMed](#)]
2. Taddeo, V.A.; Núñez, M.J.; Beltrán, M.; Castillo, U.G.; Menjívar, J.; Jiménez, I.A.; Alcamí, J.; Bedoya, L.M.; Bazzocchi, I.L. Withanolide-Type Steroids from *Physalis nicandroides* Inhibit HIV Transcription. *J. Nat. Prod.* **2021**, *84*, 2717–2726. [[CrossRef](#)] [[PubMed](#)]
3. Xu, G.-B.; Xu, Y.-M.; Wijeratne, E.M.K.; Ranjbar, F.; Liu, M.X.; Gunatilaka, A.A.L. Cytotoxic Physalins from Aeroponically Grown *Physalis acutifolia*. *J. Nat. Prod.* **2021**, *84*, 187–194. [[CrossRef](#)] [[PubMed](#)]
4. Xiang, K.; Li, C.; Li, M.X.; Song, Z.-R.; Ma, X.-X.; Sun, D.-J.; Li, H.; Chen, L.-X. Withanolides isolated from *Tubocapsicum anomalum* and their antiproliferative activity. *Bioorg. Chem.* **2021**, *110*, 104809. [[CrossRef](#)] [[PubMed](#)]
5. Wu, J.; Zhang, T.; Yu, M.; Jia, H.; Zhang, H.; Xu, Q.; Gu, Y.; Zou, Z. Anti-inflammatory Withanolides from *Physalis Minima*. *ACS Omega* **2020**, *5*, 12148–12153. [[CrossRef](#)]
6. Soh, S.; Ong, W.-Y. Effect of Withanolide A on 7-Ketocholesterol Induced Cytotoxicity in hCMEC/D3 Brain Endothelial Cells. *Cells* **2022**, *11*, 457. [[CrossRef](#)]
7. Su, Y.; Zhang, F.; Wu, L.; Kuang, H.; Wang, Q.; Cheng, G. Total withanolides ameliorates imiquimod-induced psoriasis-like skin inflammation. *J. Ethnopharmacol.* **2022**, *285*, 114895. [[CrossRef](#)]
8. Wang, H.-Y.; Yu, P.; Chen, X.-S.; Wei, H.; Cao, S.-J.; Zhang, M.; Zhang, Y.; Tao, Y.-G.; Cao, D.-S.; Qiu, F.; et al. Identification of HMGCR as the anticancer target of physapubenolide against melanoma cells by in silico target prediction. *Acta Pharmacol. Sin.* **2022**, *43*, 1594–1604. [[CrossRef](#)]
9. Khanal, P.; Chikhale, R.; Dey, Y.N.; Pasha, I.; Chand, S.; Gurav, N.; Ayyanar, M.; Patil, B.M.; Gurav, S. Withanolides from *Withania somnifera* as an immunity booster and their therapeutic options against COVID-19. *J. Biomol. Struct. Dyn.* **2022**, *40*, 5295–5308. [[CrossRef](#)]
10. Yang, W.-J.; Chen, X.-M.; Wang, S.-Q.; Hu, H.-X.; Cheng, X.-P.; Xu, L.-T.; Ren, D.-M.; Wang, X.-N.; Zhao, B.-B.; Lou, H.-X.; et al. 4 β -Hydroxywithanolide E from Goldenberry (Whole Fruits of *Physalis peruviana* L.) as a Promising Agent against Chronic Obstructive Pulmonary Disease. *J. Nat. Prod.* **2020**, *83*, 1217–1228. [[CrossRef](#)]
11. Shou, P.; Li, J.; Wei, Y.; Kai, G.; Wang, F.; Zhao, H.; Yang, B. Separation and identification of tubocapsanolide MAP and tubocapsunolide A, and the structure-activity relationship of their anti-TNBC activity. *Steroids* **2020**, *164*, 108734. [[CrossRef](#)]
12. Straughn, A.R.; Kakar, S.S. Withaferin A: A potential therapeutic agent against COVID-19 infection. *J. Ovarian Res.* **2020**, *13*, 79. [[CrossRef](#)]
13. Kuang, Z.; Bai, J.; Ni, L.; Hang, K.; Xu, J.; Ying, L.; Xue, D.; Pan, Z. Withanolide B promotes osteogenic differentiation of human bone marrow mesenchymal stem cells via ERK1/2 and Wnt/ β -catenin signaling pathways. *Int. Immunopharmacol.* **2020**, *88*, 106960. [[CrossRef](#)]
14. Lem, F.F.; Yong, Y.S.; Goh, S.; Chin, S.N.; Chee, F.T. Withanolides, the hidden gem in *Physalis minima*: A mini review on their anti-inflammatory, anti-neuroinflammatory and anti-cancer effects. *Food Chem.* **2022**, *377*, 132002. [[CrossRef](#)]
15. Singh, A.; Raza, A.; Amin, S.; Damodaran, C.; Sharma, A.K. Recent Advances in the Chemistry and Therapeutic Evaluation of Naturally Occurring and Synthetic Withanolides. *Molecules* **2022**, *27*, 886. [[CrossRef](#)]
16. Xia, G.-Y.; Cao, S.-J.; Chen, L.-X.; Qiu, F. Natural withanolides, an update. *Nat. Prod. Rep.* **2021**, *28*, 705. [[CrossRef](#)]
17. Liu, Z.-H.; Yan, H.; Liu, H.-Y. Chemical Constituents and Their Bioactivities of Plants of Taccaceae. *Chem. Biodivers.* **2015**, *12*, 221–238. [[CrossRef](#)]
18. Jiang, J.; Yang, H.; Wang, Y.; Chen, Y. Phytochemical and Pharmacological Studies of the Genus *Tacca*: A Review. *Trop. J. Pharm. Res.* **2014**, *13*, 635–648. [[CrossRef](#)]
19. He, J.; Ma, R.; Li, Z.-H.; Feng, T.; Liu, J.-K. Taccachatrones A-G, Highly Oxidized Steroids from the Rhizomes of *Tacca chantrieri* and Their Cytotoxicity Assessment. *J. Nat. Prod.* **2021**, *84*, 2265–2271. [[CrossRef](#)]
20. Huang, Y.; Liu, J.K.; Mühlbauer, A.; Henkel, T. Three Novel Taccalonolides from the Tropical Plant *Tacca subflaellata*. *Helv. Chim. Acta* **2002**, *85*, 2553–2558. [[CrossRef](#)]
21. Liu, H.-Y.; Ni, W.; Xie, B.-B.; Zhou, L.-Y.; Hao, X.-J.; Wang, X.; Chen, C.-X. Five New Withanolides from *Tacca plantaginea*. *Chem. Pharm. Bull.* **2006**, *54*, 992–995. [[CrossRef](#)] [[PubMed](#)]
22. Yang, J.-Y.; Chen, C.-X.; Zhao, R.-H.; Hao, X.-J.; Liu, H.-Y. Plantagiolide F, a minor withanolide from *Tacca plantaginea*. *Nat. Prod. Res.* **2011**, *25*, 40–44. [[CrossRef](#)] [[PubMed](#)]
23. Liu, Z.-H.; Yan, H.; Si, Y.-A.; Ni, W.; Chen, Y.; Chen, C.-X.; He, L.; Zhang, Z.-Q.; Liu, H.-Y. Plantagiolides K-N, three new withanolides and one withanolide glucoside from *Tacca plantaginea*. *Fitoterapia* **2015**, *105*, 210–214. [[CrossRef](#)] [[PubMed](#)]
24. Ni, G.; Yang, H.-Z.; Fu, N.-J.; Zhang, L.-L.; Wang, M.-C.; Chen, J.; Zhang, C.-L.; Li, Y.; Chen, X.-G.; Chen, R.-Y.; et al. Cytotoxic taccalonolides and withanolides from *Tacca chantrieri*. *Planta Med.* **2015**, *81*, 247–256. [[CrossRef](#)] [[PubMed](#)]
25. Yokosuka, A.; Mimaki, Y.; Sashida, Y. Chantriolides A and B, Two New Withanolide Glucosides from the Rhizomes of *Tacca chantrieri*. *J. Nat. Prod.* **2003**, *66*, 876–878. [[CrossRef](#)]
26. Zhang, L.; Liu, J.-Y.; Xu, L.-Z.; Yang, S.-L. Chantriolide C, a New Withanolide Glucoside and a New Spirostanol Saponin from the Rhizomes of *Tacca chantrieri*. *Chem. Pharm. Bull.* **2009**, *57*, 1126–1128. [[CrossRef](#)]

27. Yen, P.H.; Chi, V.T.Q.; Kim, D.-C.; Ko, W.; Oh, H.; Kim, Y.-C.; Dung, D.T.; Thanh, N.T.V.; Quang, T.H.; Ngan, N.T.T.; et al. Steroidal Glucosides from the Rhizomes of *Tacca chantrieri* and Their Inhibitory Activities of NO Production in BV2 Cells. *Nat. Prod. Commun.* **2016**, *11*, 45–48. [[CrossRef](#)]
28. Quang, T.H.; Ngan, N.T.T.; Minh, C.V.; Kiem, P.V.; Yen, P.H.; Tai, B.H.; Nhiem, N.X.; Thao, N.P.; Anh, H.L.T.; Luyen, B.T.T.; et al. Plantagiolides I and J, Two New Withanolide Glucosides from *Tacca plantaginea* with Nuclear Factor-kappaB Inhibitory and Peroxisome Proliferator-Activated Receptor Transactivational Activities. *Chem. Pharm. Bull.* **2012**, *60*, 1494–1501. [[CrossRef](#)]
29. Yokosuka, A.; Mimaki, Y. New Glycosides from the Rhizomes of *Tacca chantrieri*. *Chem. Pharm. Bull.* **2007**, *55*, 273–279. [[CrossRef](#)]
30. Yang, Y.; Gong, Q.; Wang, W.; Mao, Y.-L.; Wang, X.-R.; Yao, S.; Zhang, H.-Y.; Tang, C.; Ye, Y. Neuroprotective and Anti-inflammatory Ditetrahydrofuran-Containing Diarylheptanoids from *Tacca chantrieri*. *J. Nat. Prod.* **2020**, *83*, 3681–3688. [[CrossRef](#)]
31. Snatzke, G. Circular Dichroism and Optical Rotatory Dispersion—Principles and Application to the Investigation of the Stereochemistry of Natural Products. *Angew. Chem. Int. Ed.* **1968**, *7*, 14–25. [[CrossRef](#)]
32. Hsieh, P.-W.; Huang, Z.-Y.; Chen, J.-H.; Chang, F.-R.; Wu, C.-C.; Yang, Y.-L.; Chiang, M.Y.; Yen, M.-H.; Chen, S.-L.; Yen, H.-F.; et al. Cytotoxic Withanolides from *Tubocapsicum anomalum*. *J. Nat. Prod.* **2007**, *70*, 747–753. [[CrossRef](#)]
33. Tiamjan, R.; Panthong, A.; Taesotikul, T.; Rujjanawate, C.; Taylor, W.C.; Kanjanapothi, D. Hypotensive Activity of *Tacca chantrieri* and Its Hypotensive Principles. *Pharm. Biol.* **2008**, *45*, 481–485. [[CrossRef](#)]
34. Wang, L.; Zhu, L.; Gao, S.; Bao, F.; Wang, Y.; Chen, Y.; Li, H.; Chen, L. Withanolides isolated from *Nicandra physaloides* protect liver cells against oxidative stress-induced damage. *J. Funct. Foods* **2018**, *40*, 93–101. [[CrossRef](#)]
35. Jadeja, R.N.; Urrunaga, N.H.; Dash, S.; Khurana, S.; Saxena, N.K. Withaferin-A Reduces Acetaminophen-Induced Liver Injury in Mice. *Biochem. Pharmacol.* **2015**, *97*, 122–132. [[CrossRef](#)]
36. Moi, P.; Chan, K.; Asunis, I.; Cao, A.; Kan, Y.W. Isolation of NF-E2-related factor 2 (Nrf2), a NF-E2-like basic leucine zipper transcriptional activator that binds to the tandem NF-E2/AP1 repeat of the beta-globin locus control region. *Proc. Natl. Acad. Sci. USA* **1994**, *91*, 9926–9930. [[CrossRef](#)]
37. Wang, A.; Wang, S.; Jiang, Y.; Chen, M.; Wang, Y.; Lin, L. Bio-assay guided identification of hepatoprotective polyphenols from *Penthorum chinense* Pursh on t-BHP induced oxidative stress injured L02 cells. *Food Funct.* **2016**, *7*, 2074–2083. [[CrossRef](#)]
38. Velichkova, M.; Hasson, T. Keap1 regulates the oxidation-sensitive shuttling of Nrf2 into and out of the nucleus via a Crm1-dependent nuclear export mechanism. *Mol. Cell. Biol.* **2005**, *25*, 4501–4513. [[CrossRef](#)]
39. Wakabayashi, N.; Itoh, K.; Wakabayashi, J.; Motohashi, H.; Noda, S.; Takahashi, S.; Imakado, S.; Kotsuji, T.; Otsuka, F.; Roop, D.R.; et al. Keap1-null mutation leads to postnatal lethality due to constitutive Nrf2 activation. *Nat. Genet.* **2003**, *35*, 238–245. [[CrossRef](#)]
40. Wang, A.; Li, D.; Wang, S.; Zhou, F.; Li, P.; Wang, Y.; Lin, L. γ -Mangostin, a xanthone from mangosteen, attenuates oxidative injury in liver via NRF2 and SIRT1 induction. *J. Funct. Foods* **2018**, *40*, 544–553. [[CrossRef](#)]
41. Liu, J.-X.; Shen, S.-N.; Tong, Q.; Wang, Y.-T.; Lin, L.-G. Honokiol protects hepatocytes from oxidative injury through mitochondrial deacetylase SIRT3. *Eur. J. Pharmacol.* **2018**, *834*, 176–187. [[CrossRef](#)] [[PubMed](#)]
42. Chen, C.; Ren, Y.; Zhu, J.; Chen, J.; Feng, Z.; Zhang, T.; Ye, Y.; Lin, L. Ainsliadimer C, a disesquiterpenoid isolated from *Ainsliaea macrocephala*, ameliorates inflammatory responses in adipose tissue via Sirtuin 1-NLRP3 inflammasome axis. *Acta Pharmacol. Sin.* **2022**, *43*, 1780–1792. [[CrossRef](#)] [[PubMed](#)]